PHOTONICS Research

Research progress in large-area perovskite solar cells

Yang Zhao,[1,2] Fei Ma,[1,2] Feng Gao,[1,2] Zhigang Yin,[1,2] Xingwang Zhang,[1,2] and Jingbi You[1,2,*]

[1]Key Laboratory of Semiconductor Materials Science, Institute of Semiconductors, Chinese Academy of Sciences, Beijing 100083, China
[2]College of Materials Science and Opto-electronic Technology, University of Chinese Academy of Sciences, Beijing 100049, China
*Corresponding author: jyou@semi.ac.cn

Received 19 March 2020; revised 19 April 2020; accepted 21 April 2020; posted 21 April 2020 (Doc. ID 392996); published 1 July 2020

The record power conversion efficiency of small-area perovskite solar cells has impressively exceeded 25%. For commercial application, a large-area device is the necessary next step. Recently, significant progress has been achieved in fabricating efficient large-area perovskite solar cells. In this review, we will summarize recent achievements in large-area perovskite solar cells including the deposition methods as well as growth control of the large-area, high-quality perovskite layer and also the charge transport layer. Finally, we will give our insight into large-area perovskite solar cells.

https://doi.org/10.1364/PRJ.392996

1. INTRODUCTION

Inorganic-organic hybrid perovskite solar cells (PSCs) have been one of the brightest spotlights in the photovoltaic research field in recent years. Their power conversion efficiency (PCE) has risen from 3.9% to 25.2% since 2009 [1–9], which surpasses the most effective thin-film solar cells such as CuInGaSe (CIGS) and CdTe and could be comparable with crystal silicon solar cells [10]. This remarkable progress is due to its excellent optoelectronic properties: excellent light absorption coefficient ($\approx 10^5$ cm^{-1}), long carrier diffusion lengths (>1 μm), and high defect tolerance [11]. Despite these impressive achievements, most high PCEs of PSCs are recorded on small areas and fabricated by spin-coating methods, typically around 0.1 cm^2 [12–14].

When considering commercial application, it is necessary to fabricate large-area PSCs. The area of most modules is greater than or equal to 1 cm^2 and less than or equal to 800 cm^2. According to different substrate materials, large-area PSCs can be divided into rigid and flexible types. So far, the champion cell efficiency of the flexible cell is 19.11% [15], and the world-best efficiency for a flexible perovskite module is about 15% with an area of 30 cm^2 [16]. To date, there are also significant progress in rigid large-area device fabrication.

For example, Han *et al.* attempted to fabricate 1 cm^2 large-area perovskite solar cells by traditional spin coating in 2015 via heavily doped inorganic charge extraction layers in PSCs, and a PCE > 15% in 1 cm^2 cells was obtained [17]. In 2017, Sargent and co-workers used chlorine-capped TiO_2(Cl-TiO_2) films as an electron transport layer, which suppressed interface nonradiative recombination in solution-processed PSCs. A certified PCE of 19.5% for active areas of 1.1 cm^2 was achieved [18]. In the same year, Seok *et al.* reported that the introduction of excessive iodide ions into the solution of perovskite, which through an intramolecular exchange process formed the perovskite layers and decreased the concentration of deep-level defects, resulted in obtaining a certified PCE of 19.7% in 1 cm^2 [6]. Later, our group reported a 1 cm^2 perovskite solar cell with efficiency of 20.1% by optimization of grain boundary passivation with PbI_2 [19].

However, it is a crucial challenge to produce a large-area device with an area larger than 5 cm × 5 cm by using a conventional spin-coating method. Several scalable deposition techniques have been developed to prepare perovskite films, such as doctor blading, inkjet printing, and slot-die coating. Some progressed have also been made in preparing large-area PSCs by these methods. For example, in 2015, by using bladed $MAPbI_3$ films, a maximum PCE of 15.1% in approximately 6.45 cm^2 substrates was achieved. In 2018, through adding L-α-phosphatidylcholine in perovskite ink, the blading coating rate was controlled, and a smoother perovskite film was obtained, resulting in stabilized module PCE of 15.3% and 14.6% measured at aperture areas of 33.0 cm^2 and 57.2 cm^2, respectively [20,21]. In 2017, Han *et al.* reached a certified PCE of 12.1% with an aperture area of 36.1 cm^2 by a pressure-processing method for the deposition of perovskite films [22].

In addition to the above-mentioned published results, some companies have also achieved good results in developing large-area PSCs. In 2019, Microquanta Semiconductor reported large-area perovskite modules (about 20 cm^2) with a PCE of 18.04% [23]. A PCE of 16.1% was also reported by Panasonic for a submodule (55 series cells) with an area of 802 cm^2 [24]. The efficiency for flexible PSCs with single junctions for large-area

modules reported by Toshiba and Nedo stands at 11.7% with an area of 703 cm^2 [25].

In this mini-review, we will briefly summarize the progress in large-area perovskite solar cells, including optimization of the deposition method as well as growth control of the large-area, high-quality of perovskite layer and also the charge transport layer (CTL). Finally, a perspective of PSCs is also included.

2. DEPOSITION METHODS OF LARGE-AREA PEROVSKITE SOLAR CELLS

At present, PSCs can be divided into rigid and flexible PSCs, according to different substrate materials used to prepare large-area PSCs. Large-area solar cell fabrication technologies [such as doctor-blade coating, slot-die coating, inkjet printing, and roll to roll (R2R)] can be used not only to manufacture flexible PSCs but also to produce rigid PSCs. Next, we briefly summarize these methods for preparing large-area PSCs.

A. 1 cm^2 Device by Spin Coating

Spin coating has been widely used to fabricate small PSCs (~0.1 cm^2) and large devices with area of 1 cm^2 as well. The main advantage of the spin-coating method is that the preparation method is simple, and the chemical component and the thickness of the perovskite film can be easily controlled.

The spin-coating method includes one-step and two-step spin-coating methods. The preparation process of spin coating is shown in Figs. 1(a) and 1(b) [26]. For one-step spin coating, briefly, the halide organic salt [e.g., methylammonium iodide (MAI), formamidinium iodide (FAI)] and lead halide (PbI_2, $PbBr_2$, or their mixture) powders are mixed and dissolved in a solvent such as N,N-dimethylformamide (DMF) or dimethyl sulfoxide (DMSO). The mixed solution is spun on the CTL of electrons or holes, and the perovskite films were formed after annealing. In 2015, Chen *et al.* published in *Science* the most compelling report for large-area PSCs [Fig. 1(c)]. This work is prepared using n-i-p structure PSCs, using Nb-doped TiO_2 as the electron transport layer (ETL) and Li-Mg-co-doped NiO as the hole transport layer (HTL) in planar PSCs. Meanwhile, using one-step deposition of a PbI_2/MAI mixture, a certified efficiency of 15% with the device area of 1.02 cm^2 was reported [17].

For the two-step spin-coating method, lead halide and halide organic salt powders are dissolved in DMF and isopropanol (IPA), respectively. First, the lead halide solution is spin coated on the ETL/HTL, and then it is annealed. Subsequently, the MAI solution is spin coated on lead halide surface, and the perovskite films are obtained after annealing by interdiffusion. In 2018, You *et al.* obtained 1 cm^2 perovskite solar cells with the efficiency of 20.1% by two-step spin coating and controlled the residual PbI_2 on the perovskite surface [Fig. 1(d)] [19].

For the spin-coating method, the disadvantage is that the material utilization rate is too low, and it is difficult to form a pinhole-free and uniform perovskite film on a larger area of the substrates, so it is not conducive to preparing large perovskite films (>1 cm^2). The spin-coating method for preparing perovskite layers is mostly done in an inert gas glove box, where different types of perovskite components can be selected. But the preparation of larger perovskite layers by methods such as doctor-blade coating and spray coating needs to be performed in air. $MAPbI_3$ precursor solution is mostly used to prepare larger-area perovskite layers due to its more stable structure at room temperature, while $FAPbI_3$ and $CsPbI_3$ perovskite phases (α-$FAPbI_3$ and α-$CsPbI_3$) are unable to be used at room temperature and easily transformed into nonperovskite phases (δ-$FAPbI_3$ and δ-$CsPbI_3$) through thermodynamic phase transformation [27].

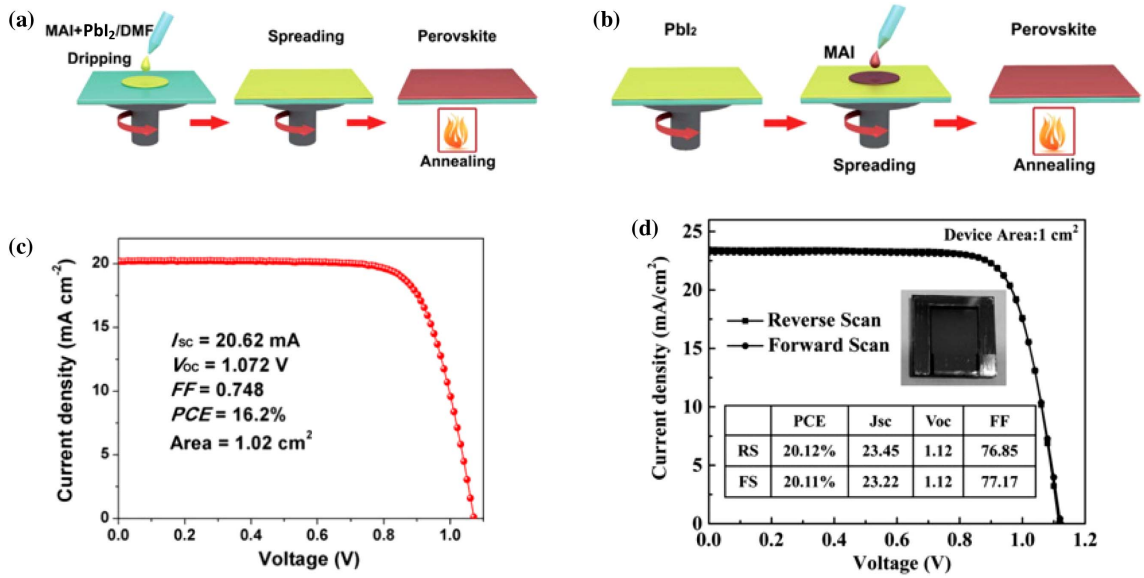

Fig. 1. (a) One-step deposited perovskite films. (b) Two-step deposited perovskite films. (c) J-V curve of the best large cell endowed with anti-reflection film. (d) J-V curve of the PSCs in large size of 1 cm^2 measured under reverse and forward scan under one-sun condition. (a), (b) Reproduced with permission [26], Copyright 2018, Royal Society of Chemistry. (c) Reproduced with permission [17], Copyright 2015, American Association for the Advancement Science. (d) Reproduced with permission [19], Copyright 2017, Nature Publishing Group.

B. Blade Coating

The first attempt to replace spin coating in the processing of large-area PSCs was the blade-coating method. Blade coating has been widely used for large-area film deposition due to its high material utilization and fast R2R process [24]. Figure 2(a) shows the setup for the blade-coating technique for fabricating perovskite films onto substrates. Specifically, a perovskite precursor solution was dropped onto CTL covered transparent conductive electrode (TCO) substrates, and it was swiped linearly by a glass blade with a suitable speed [28]. The thickness of the perovskite films during doctor-blade coating was controlled by the perovskite precursor solution concentration, the blading speed, and the spacing of the doctor blade and the substrates.

Compared with the spin-coating process, the solvent evaporation rate of the perovskite film coated by the blade is relatively slow, which facilitates the growth of larger crystals, but it is difficult to form a dense film through the natural drying process. To address this issue, in 2018 Huang *et al.* bladed a perovskite precursor solution (ink) over a preheated substrate (typically ~ 70–145°C). As the solvent evaporates, the perovskite precursor material crystallizes into black solid perovskite films. The preheating of the substrates can speed up blade coating and suppress the formation of needle-like structures in the perovskite films [Fig. 2(a)] [21]. In 2019, Huang *et al.* reported a method to accelerate liquid layer drying at room temperature by introducing a nitrogen knife (N_2 knife) after a fixed distance blade and applying a nitrogen flow [Figs. 2(b) and 2(c)]. A 2% volatile noncoordinating solvent (VNCS) is introduced into nonvolatile coordinating solvent (NVCS) to dissolve the perovskite powder, which can achieve rapid drying at room temperature, but also achieve larger perovskite grains. Finally, a certified PSC module with an efficiency of 16.4% and an area of 63.7 cm^2 was obtained [29].

For blade coating, the biggest challenge in preparing large-area PSCs may be forming perovskite films without pinholes. Therefore, the perovskite precursor solution is very important for preparing a perovskite thin film by the blade-coating method.

C. Slot-Die Coating

Slot-die coating [Fig. 3(a)] is similar to blade coating, that is, it uses a continuously supplied ink reservoir with a thin slit to apply ink over the substrate. However, slot-die coating shows better yield and reproducibility than blade coating when the ink is already fully developed. Thus, it has more potential to be applied in both sheet-to-sheet (S2S) and R2R coating fabrication in the future [30].

Several attempts have been made to apply the slot-die coating technique to fabricate large-area PSCs on both flexible and rigid substrates. In 2015, slot-die coating was first applied to fabricate large-area PSCs, with a device configuration of ETL(ZnO)/$MAPbI_3$/HTL (P3HT), using an air knife to dry the wet film. First, a uniform PbI_2 layer was formed by N_2 gas quenching assisted slot-die coating, and then MAI solution was dipped onto PbI_2 and converted into a perovskite film. In addition to the perovskite layer, the inorganic ZnO and polymeric P3HT were also coated using the slot-die coating. The temperature of the substrate and air knife also influence the resulting film morphology and photoelectric performance. After optimization of coating speed and substrate temperature, a PCE of 11.96% was obtained for the size of 0.1 cm^2 [Figs. 3(b) and 3(c)] [31,32]. In 2018, Gao and co-workers

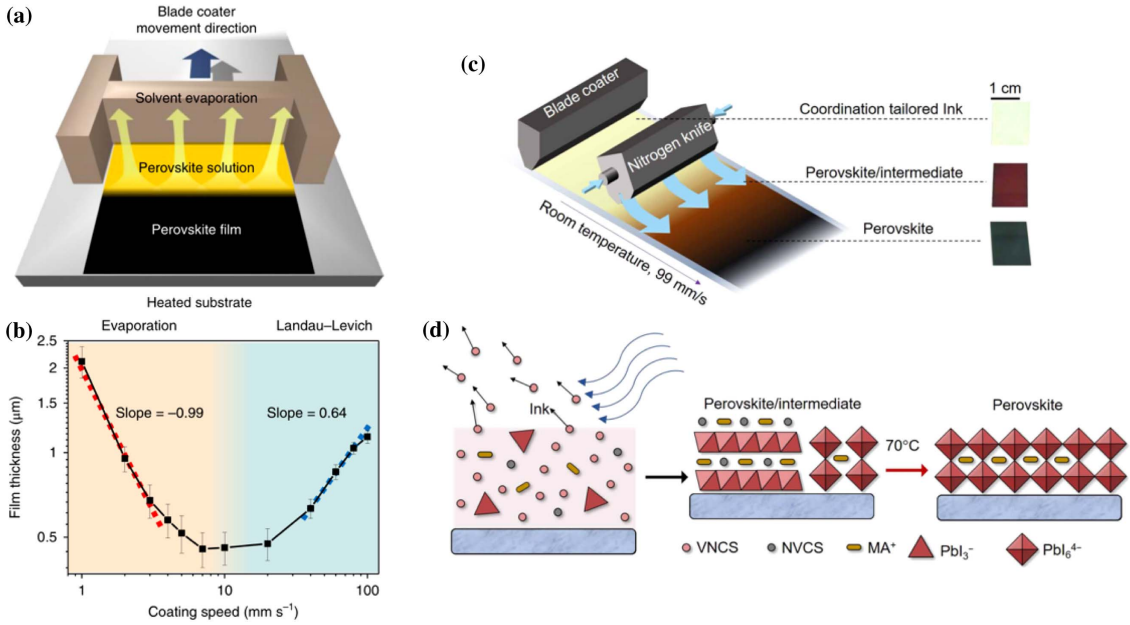

Fig. 2. (a) Schematic illustration for the blade coating of perovskite film in the Landau–Levich mode. (b) The perovskite film's thickness as a function of blade-coating speed by coating a 1 mol/L $MAPbI_3$/DMF solution on a 145°C preheated substrate. (c) Schematic illustration for N_2-knife-assisted blade coating of perovskite films. (d) Schematic illustration showing the drying of ink into a perovskite/intermediate film and full crystallization of a perovskite film. VNCS, volatile noncoordinating solvent; NVCS, nonvolatile coordinating solvent. (a) Reproduced with permission [21], Copyright 2018, Nature Publishing Group. (b)–(d) Reproduced with permission [29], Copyright 2019, American Association for the Advancement Science.

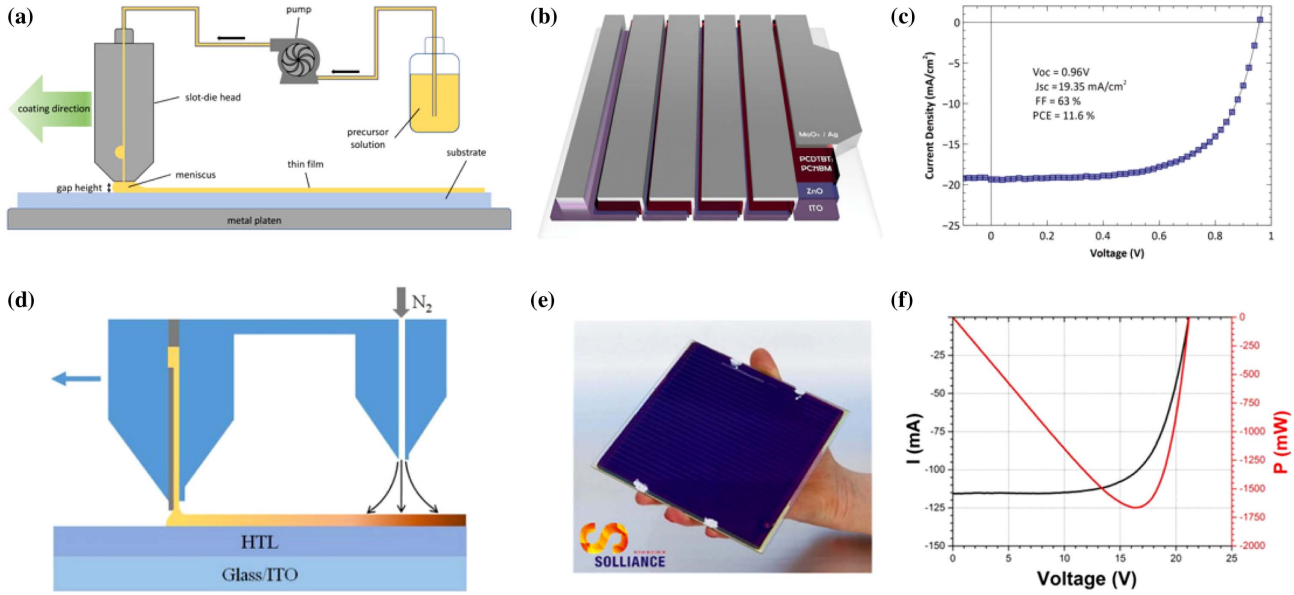

Fig. 3. (a) Schematic illustration of the key steps involved in slot-die coating of perovskite thin films. (b) and (c) Schematic drawing of a module and J-V curve of an organometal halide perovskite solar cell, respectively. (d) The slot-die coating process for preparing $CH_3NH_3PbI_3$ films. (e) and (f) 15.24 cm × 15.24 cm perovskite module and I-V curve, respectively. (a) Reproduced with permission [30], Copyright 2018, Royal Society of Chemistry. (b) and (c) Reproduced with permission [31], Copyright 2014, Wiley. (d) Reproduced with permission [33], Copyright 2018, Elsevier. (e) and (f) Reproduced with permission [34], Copyright 2018, Elsevier.

added 10 mg · mL^{-1} NH_4Cl into the perovskite solution, where PCEs of 15.57% was obtained using the slot-die coating processes [Fig. 3(d)] [33]. In the same year, Galagan and co-workers, with utilization of the slot-die coating process, demonstrated 168.75 cm^2 and 149.5 cm^2 PSCs [Fig. 3(e)] with PCEs of 11.1% and 11.8%, respectively [Fig. 3(f)] [34].

Notwithstanding these potential advantages, there are still numerous challenges that must be overcome in order to obtain continuous and stable thin perovskite films for high-efficiency large-area PSCs, such as preparing the appropriate perovskite ink and selecting the appropriate blade knife.

D. Spray Coating

Spray coating is a low-temperature coating technology that is suitable for scale-up and is a widely used deposition technique in industry. Its advantages are that it can manufacture PSCs devices with low cost, high volume, rapid manufacturing, and high material utilization. Spray coating generally relies on the use of relatively low-concentration "inks." The solvent evaporates to dry the ink to produce a film of the desired thickness, which is in stark contrast to the use of blade coatings and slot-die coatings to make films.

Spray-coating processes can be broken down into four stages [Fig. 4(a)]: (i) the generation of the ink droplets, (ii) the transport of the droplets to the substrate, (iii) the coalescence of the droplets into a wet film, and (iv) the drying of the thin film [35].

In recent years, researchers have also made some progress in the preparation of PSCs by the spray-coating method. For example, in 2014, Barrows *et al.* reported a method for manufacturing planar heterojunction $CH_3NH_3PbI_{3-x}Cl_x$ PSCs using ultrasonic spraying as a deposition technique under environmental conditions, forming an active layer in an inverted structure PV device (p-i-n) and achieving peak PSCs with a PCE of 11%. They found that the temperature of the substrate during spraying, the volatility of the solvent, and the post-deposition annealing temperature all determined the efficiency of the PSCs [36]. In 2016, Tait *et al.* further improved the efficiency of PSCs based on $CH_3NH_3PbI_xBr_{3-x}$ with an active area of 3.8 cm^2 to 11.7% by quickly and accurately optimizing the precursor ratio [Fig. 4(b)] [35]. In the same year, Im and co-workers, by controlling the redissolution and crystal grain growth of the $MAPbI_{3-x}Cl_x$ mixed halide perovskite film via spray coating, fabricated a submodule (10 cm × 10 cm, active area 40 cm^2) with a PCE of 15.5% [37]. In 2018, Choi *et al.* applied megasonic spray coating to the fabrication of large-area PSCs (1 cm^2), with a PCE of 14.2% [Figs. 4(c) and 4(d)] [38].

As with other technologies, the use of spraying also faces similar challenges, that is, the crystallization of the perovskite itself must be controlled to form a high-quality perovskite film in order to obtain higher efficiency and more stable large-area PSCs.

E. Inkjet Printing

Inkjet printing is familiar to most people in the form of desktop office printers and is widely used commercially. The main processing advantages of this method are that it can scale from laboratory scale to large-scale production with low cost and low material consumption. Its working principle is to eject the precise deposition and fixation on the ink substrate in the form of droplets from the nozzle. The two most common approaches are shown in Figs. 5(a) and 5(b): (i) continuous inkjet printing (CIP) and (ii) drop-on-demand (DOD) inkjet printing [39,40].

Since the advent of PSCs, great progress has been made in the preparation of large-area PSCs by inkjet printing. In 2016, Mhaisalkar *et al.* completed the upgrade of PSC modules

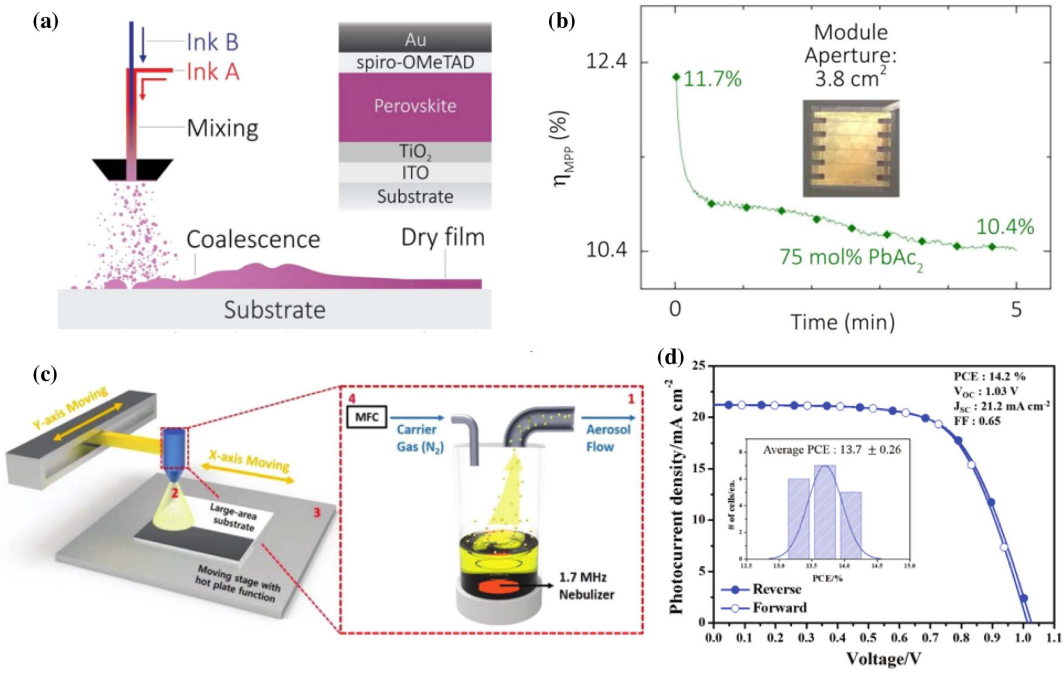

Fig. 4. (a) Schematic of concurrently pumped ultrasonic spray coating for perovskite precursor deposition. (b) A spray-coated four-cell module (3.8 cm^2) from the 75% (molar fraction) $PbAc_2$ with $PbCl_2$. (c) and (d) Schematic representation of the megasonic spray-coating process and J-V curves of perovskite solar cells, respectively. (a) and (b) Reproduced with permission [35], Copyright 2016, Royal Society of Chemistry. (c) and (d) Reproduced with permission [38], Copyright 2018, Wiley.

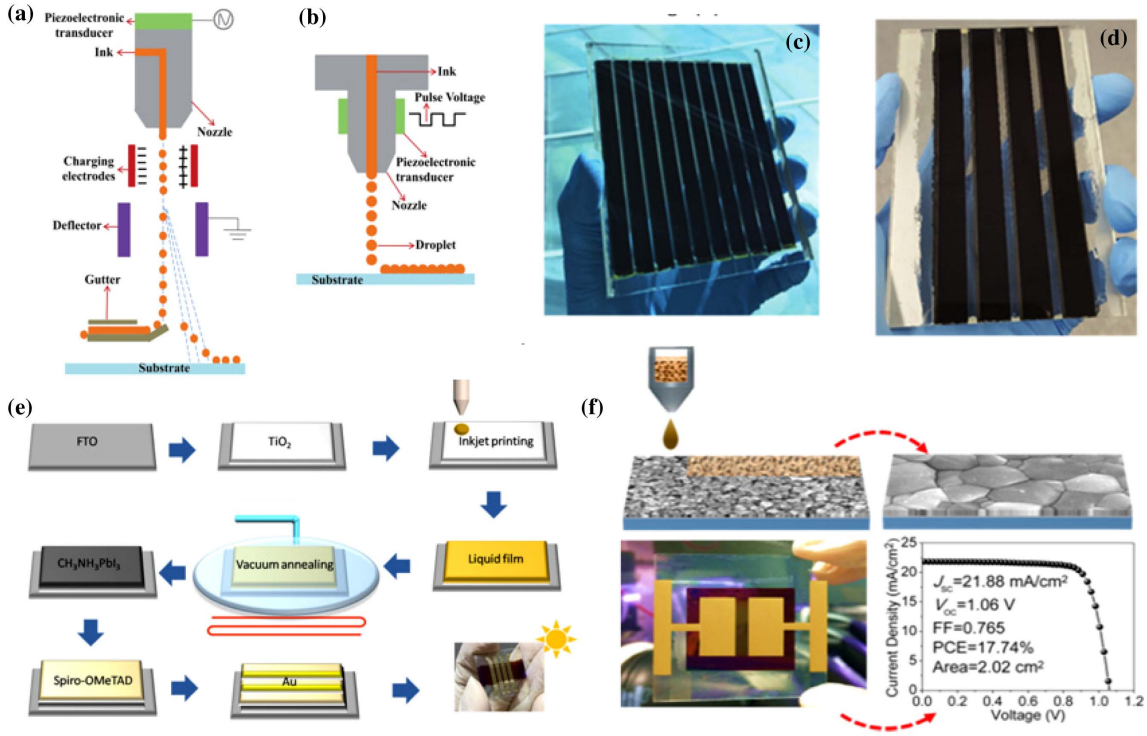

Fig. 5. Schematic diagrams for the two main inkjet-printing methods: (a) continuous inkjet printing (CIJ); (b) drop-on-demand (DOD) inkjet printing. (c) 10 cm × 10 cm device and (d) 10 cm × 5 cm device. (e) Schematic illustration of PSC fabrication through inkjet printing with vacuum annealing. (f) J–V curves of PSCs on inkjet printing with active area 2.02 cm^2. (a) and (b) Reproduced with permission [40], Copyright 2019, Wiley. (c) and (d) Reproduced with permission [41], Copyright 2016, Royal Society of Chemistry. (e) Reproduced with permission [42], Copyright 2018, Wiley. (f) Reproduced with permission [43], Copyright 2018, Elsevier.

under high-efficiency and stable conditions using solution processing and low-cost electrode materials. Monolithic perovskite modules of size 10 cm × 10 cm (active area 70 cm^2) and 10 cm × 5 cm (active area 31 cm^2) with PCEs of 10.74% and 10.46% were obtained, respectively [Figs. 5(c) and 5(d)] [41]. In 2018, Xing *et al.* demonstrated that high-quality perovskite films could be inkjet printed by innovative vacuum-assisted thermal annealing post-treatment and optimized solvent composition.

High-performance PSCs based on printed $CH_3NH_3PbI_3$ with a PCE of 13.27% for 4.0 cm^2 was demonstrated [Fig. 5(e)] [42]. In the same year, Song *et al.* used a two-step printing method and designed a PbI_2 ink precursor with a different solvent composition, and then they used MAI vapor as a reactant to convert PbI_2 to $MAPbI_3$, which resulted in a PSC with an area of 2.02 cm^2 and a PCE of 17.74% [Fig. 5(f)] [43].

Although some achievements have been made, there are also some challenges in the production of high-efficiency large-area PSCs by the inkjet printing method, for example, the development of printable perovskite inks and durability of the print head.

F. Roll to Roll

R2R printing technology is a method for preparing large-area PSCs. Compared with other preparation methods, its preparation speed is very fast, and its cost is the most competitive. At present, the continuous R2R process is being used to prepare PSCs on flexible substrates.

In 2018, Gao *et al.* developed blowing-assisted drop-casting (BADC) in conjunction with an NH_4Cl additive to prepare $MACH_3NH_3PbI_3$ films in air. The NH_4Cl additive was critical to form high-quality perovskite films. The optimized formulation is then successfully applied to R2R on a flexible substrate, giving a record PCE of 11.16% with an area of 6.25 cm^2 [Fig. 6(a)] [34]. In 2019, a nonelectroactive polymer [polyethyleneimine ethoxylate (PEIE)] was used in perovskite to significantly improve its humidity tolerance by Kim *et al.* They also reported a hot slot-die coating method that can be used for the fabrication of PSCs via an R2R process in air. By optimizing the preparation process, they obtained a flexible perovskite solar cell with a photoelectric conversion efficiency of 11.7% [Fig. 6(b)] [44]. In the same year, gravure printing was successfully applied for the fabrication of flexible PSCs for the first time by Seo *et al.* A PCE of 9.7% was achieved for partly R2R processed PSCs based on a two-step fabrication of the perovskite layer [Fig. 6(c)] [45].

G. Other Novel Approaches

In addition to the above-mentioned classic preparation methods, in order to improve the efficiency of large-area PSCs, researchers have also improved the preparation methods and developed some novel preparation methods to fabricate high-quality perovskite. For example, in 2016, Grätzel *et al.* used a vacuum-flash-assisted solution process to fabricate high-efficiency large-area PSCs; an illustration of the nucleation/crystallization procedures during the formation of perovskite film via vacuum-flash-assisted solution processing is shown in Fig. 7(a). This method enabled them to fabricate perovskite films with larger grain size than those created through the conventional processes [Fig. 7(b)]. By this method, they obtained PSCs with a maximum PCE of 20.5% and a certified PCE of 19.6% with an area of more than 1 cm^2 [46]. In 2017, the pressure-processing method for the deposition of perovskite films was used by Han *et al.* They applied pressure via a pneumatically driven squeezing board, which spread the liquid precursor under the PI film [Figs. 7(c) and 7(d)]. The pressure was held for 60 s and then unloaded. The assembly was put on a hotplate at 50°C for 2 min. After peeling off the PI film at a speed of 50 $mm \cdot s^{-1}$, a dense and uniform perovskite film with a larger grain size was formed in air at room temperature.

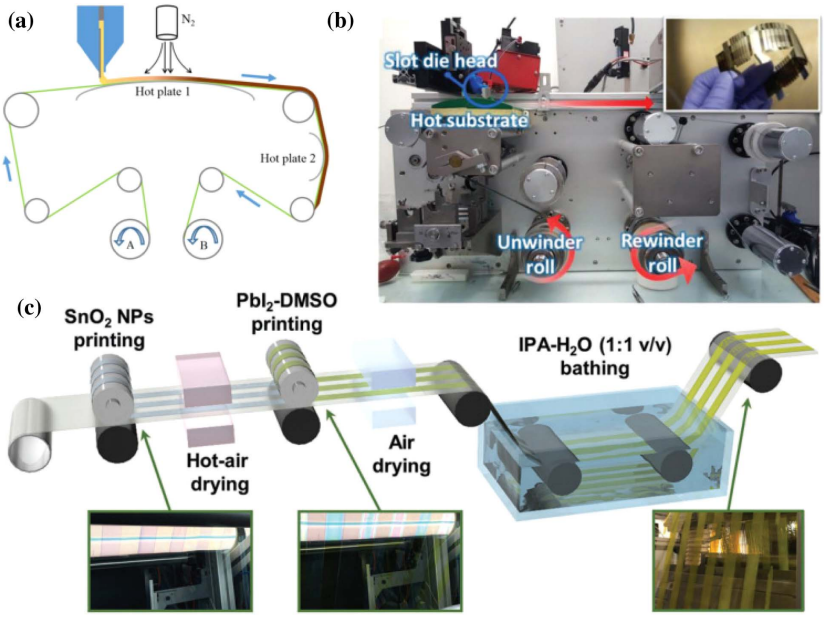

Fig. 6. (a)–(c) Roll-to-roll processing setup for continuous preparation of perovskite solar cells. (a) Reproduced with permission [34], Copyright 2018, Elsevier. (b) Reproduced with permission [44], Copyright 2019, Wiley. (c) Reproduced with permission [45], Copyright 2019, Wiley.

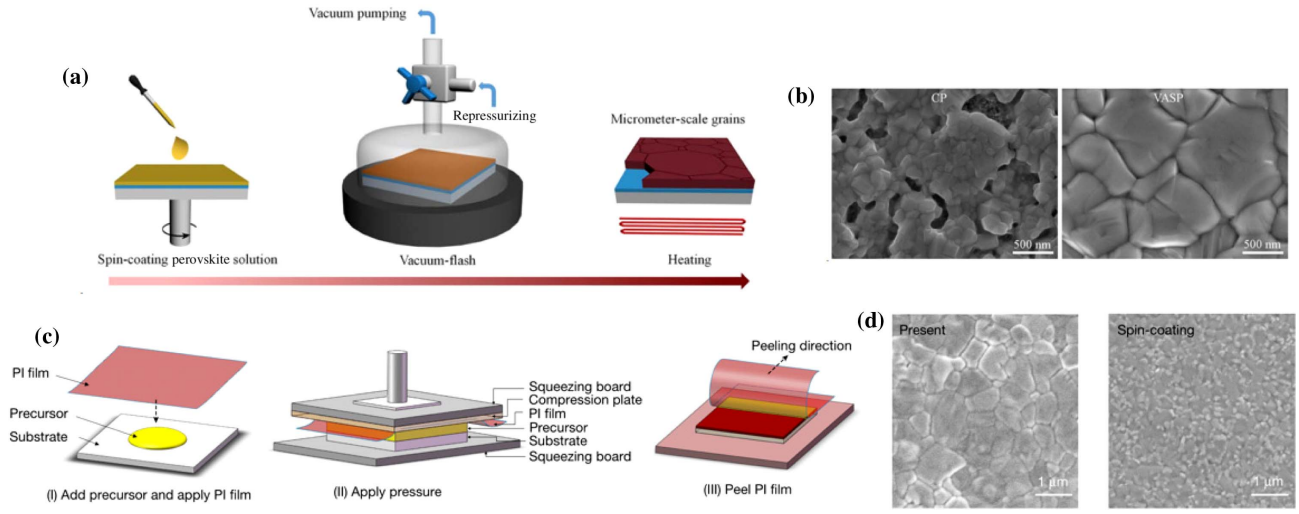

Fig. 7. (a) Schematic illustration of vacuum-flash-assisted solution processing (VASP). (b) Surface scanning electron microscope (SEM) images of the perovskite films fabricated by the conventional process and vacuum-assisted solution process. (c) Diagram of the pressure-processing method for the deposition of perovskite films. (d) Surface SEM images of the perovskite films fabricated by the pressure-processing method and spin coating. (a) and (b) Reproduced with permission [20], Copyright 2015, Royal Society of Chemistry. (c) and (d) Reproduced with permission [46], Copyright 2016, American Association for the Advancement of Science.

They achieved a certified PCE of 12.1% with an aperture area of 36.1 cm^2 for a mesoporous TiO_2-based perovskite solar module architecture [20]. The photovoltaic performance of large-area PSCs prepared by different methods is summarized in Table 1.

3. GROWTH OF HIGH-QUALITY LARGE-AREA PEROVSKITE FILMS

Although there are many works for fabricating large-area PSCs, their efficiency still lags behind that of those small-area devices that are fabricated by spin coating (Fig. 8) [47]. No matter which method is used to prepare large-area PSCs, the preparation of high-quality perovskite films is the key factor to further improve the efficiency of PSCs [48]. The following is a brief summary of current methods for improving the quality of perovskite films for large-area PSCs and the photovoltaic performance of large-area PSCs with different additive strategies will be summarized in Table 2.

A. Solvent Engineering

Solvents that dissolve or process perovskite precursors often show different boiling points and polarities. These will affect the crystallization process.

N, N-dimethylformamide (DMF) is widely used as a solvent for the preparation of PbI_2 or perovskite precursor. When it is used only as a solvent, it will lead to rapid crystallization of PbI_2 or perovskite, and a poor-quality perovskite film will be formed, which severely affects the efficiency of the PSCs. To solve this problem, researchers have done a lot of outstanding work. In 2014, Han *et al.* and Seok *et al.* used the strongly coordinative solvent DMSO as solvent or as additive in PbI_2 or a perovskite precursor to obtain a highly uniform perovskite film with no residual PbI_2 owing to the formation of a PbI_2–DMSO complex [49,50]. In 2017, You *et al.* added 5% volume of DMSO solvent in DMF as a mixture solvent for dissolving PbI_2 beads. The obtained PbI_2 layer with DMSO additive is dense and smooth, the morphology of the formed perovskite layer has also

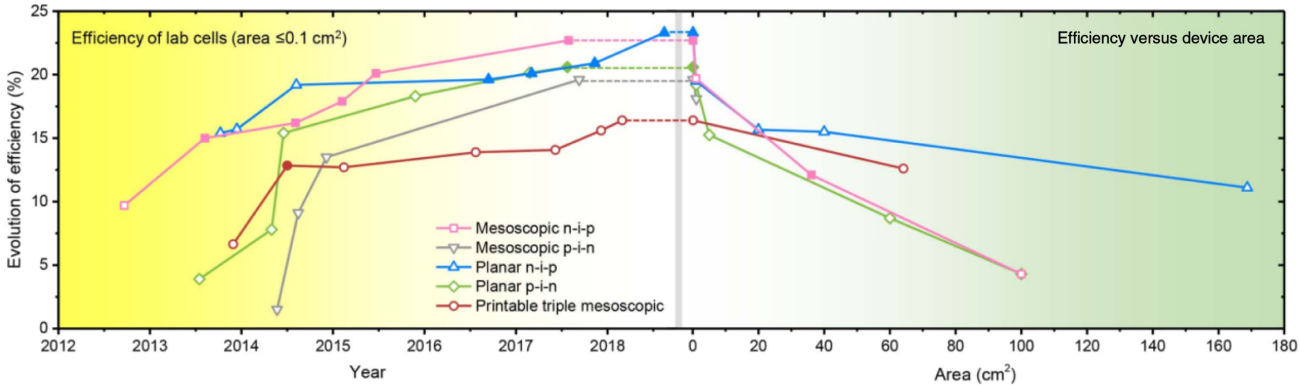

Fig. 8. Evolution of the best reported lab-cell (≤0.1 cm^2) efficiencies and large-area (≥1.0 cm^2) device efficiencies. Reproduced with permission [47], Copyright 2018, American Association for the Advancement of Science.

Table 1. Photovoltaic Performance of Perovskite Solar Cells Prepared by Different Methods

Deposition Method	Device Structure	Device Area (cm^2)	PCE (%)	J_{sc} ($mA \cdot cm^{-2}$)	V_{oc} (V)	FF (%)	Reference
Spin coating	FTO/NiMgLiO/$MAPBI_3$/PCBM/Ti(Nb)O_x/Ag	1.02	16.2	20.21	1.072	74.8	[17]
Spin coating	ITO/SnO_2/$(FAPbI_3)_{1-x}(MAPbBr_3)_x$/Spiro-OMeTAD/Au	1	20.12	23.45	1.12	76.85	[19]
Blade coating	ITO/PEDOT:PSS/$CH_3NH_3PbI_xCl_{3-x}$/PC_{61}BM/Bis-C_{60}/Ag	—	10.44	16.73	0.96	65.0	[28]
Blade coating	ITO/PTAA/$MAPbI_3$/C_{60}/BCP/Cu	33.0	15.0	19.5	1.07	72.1	[21]
		57.2	15.0	20.3	1.07	68.9	
Blade coating	ITO/PTAA/$MAPbI_3$/C_{60}/BCP/Cu	63.7	16.9	74.5 (mA)	18.9	76.2	[21]
Slot-die coating	PET/ITO/SnO_2/perovskite/Spiro-OMeTAD/Au	30	14.47	3.3	6.54	67.0	[16]
Slot-die coating	ITO/SnO_2/$MAPbI_3$/Spiro-OMeTAD/Au	1	18.0	21.5	1.10	76.0	[30]
Slot-die coating	ITO/ZnO/$MAPbI_3$/doped-P3HT/Ag	0.1	11.6	19.35	0.96	63.0	[31]
		47.3	4.57	—	—	—	
Slot-die coating	ITO/ZnO/$MAPbI_3$/doped-P3HT/Ag	0.1	11.96	20.38	0.98	60.0	[32]
Slot-die coating	ITO/PEDOT:PSS/$MAPbI_3$/PC_{61}BM/Ca/Ag	0.1	15.75	19.79	1.02	77.15	[33]
Slot-die coating	ITO/TiO_2/$CH_3NH_3PbI_{3-x}Cl$/Spiro-MeOTAD/Au	168.75	11.1	0.69	21.2	68.0	[34]
		149.5	11.8	0.76	20.8	71.0	
Spray coating	ITO/PEDOT:PSS/$MAPbI_3$/PCBM/Ca/Al	0.025	11.1	16.8	0.92	72.0	[36]
Spray coating	FTO/TiO_2/$MAPbI_{3-x}Cl_x$/PTAA/Au	40	15.5	84.1 (mA)	10.5	70.16	[37]
Spray coating	ITO/TiO_2/$MAPbI_3$/Spiro-MeOTAD/Au	3.8	11.7	19.4	3.31	70.0	[35]
Spray coating	ITO/PEDOT:PSS/$MAPbI_3$/C_{60}/BCP/Cu	1	14.2	21.3	1.03	65.0	[38]
Inkjet printing	FTO/TiO_2/ZrO_2/carbon/perovskite	31	10.46	19.6	3.72	57.5	[41]
	(drop casted perovskite through carbon layer)	70	10.75	17.72	9.63	62.9	
Inkjet printing	FTO/TiO_2/5 nm C_{60}/$MAPbI_3$/Spiro-MeOTAD/Au	4	13.24	20.4	1.04	62.57	[42]
Inkjet printing	FTO/c-TiO_2/m-TiO_2/$MAPbI_3$/Spiro-MeOTAD/Au	2.02	17.74	21.88	1.06	76.5	[43]
Roll-to-roll	ITO/m-PEDOT:PSS/$CH_3NH_3PbI_3$/PCBM/Ca/Al	6.25	11.16	17.39	0.99	64.82	[34]
Vacuum-flash-assisted solution process	FTO/c-TiO_2/m-TiO_2/$FA_{0.81}MA_{0.15}PbI_{2.51}Br_{0.45}$/Spiro-MeOTAD/Au	1	20.38	23.19	1.143	76.0	[46]
Pressure-processing method	FTO/c-TiO_2/m-TiO_2/$MAPbI_3$/Spiro-MeOTAD/Au	36.1	15.7	71.1	10.5	75.7	[22]

Table 2. Photovoltaic Performance of Perovskite Solar Cells Prepared by Using Different Materials as Additives for Perovskite Layers

Materials	Perovskite Components	Device Area (cm^2)	PCE (%)	J_{sc} ($mA \cdot cm^{-2}$)	V_{oc} (V)	FF (%)	Reference
DMSO	$(FAPbI_3)_{1-x}(MAPbBr_3)_x$	1	20.12	23.45	1.12	76.85	[19]
Nonvolatile coordinating solvents (2-methoxyethanol and acetonitrile)	$MAPbI_3$	63.7	16.9	18.9	74.5	76.2	[29]
MACl, $PbCl_2$	$MAPbI_{3-x}Cl_x$	1	15.4	21.0	1.06	69.1	[51]
		25	12.0	2.6	0.798	58.2	
MACl	$MAPbI_3$	1.2	17.33	21.38	1.11	72.9	[52]
MACl	$MAPbI_3(Cl)$	25	15.3	3.66	6.65	63.0	[53]
MAI	$MAPbI_3$	1.2	15.3	21.3	1.09	66.1	[54]
$PbCl_2$	$MAPbI_{3-x}Cl_x$	4	13.6	19.9	0.91	75.0	[55]
KI	$K_x(Cs_{0.05}(FA_{0.85}MA_{0.15})_{0.95}Pb(I_{0.85}Br_{0.15})_3$	20	15.76	3.57	6.79	65.0	[56]
CsBr	$Cs_{0.1}FA_{0.9}PbI_{2.9}Br_{0.1}$	91.8	9.34	1.16	13.55	59.6	[57]
L-α-phosphatidylcholine	$MAPbI_3$	33	15.0	19.5	1.07	72.1	[21]
		57.2	15.0	20.3	1.07	68.9	
1,8-diiodooctane (DIO)	$CH_3NH_3PbI_{3-x}Cl_x$	—	10.3	15.6	0.92	71.0	[58]
1,8-diiodooctane (DIO)	$CH_3NH_3PbI_{3-x}Cl_x$	12	11.2	6.48	2.71	63.8	[59]
I_3^-	$(FAPbI_3)_x(MAPbBr_3)_{1-x}$	1	19.7	24.7	1.10	72.3	[6]
PbI_2	$(FAPbI_3)_{1-x}(MAPbBr_3)_x$	1	20.12	23.45	1.12	76.85	[19]

been improved, and an efficiency of 20.1% in 1 cm^2 has been achieved by using the two-step spin-coating fabrication method [18]. When larger-area PSCs are prepared by other methods, at very fast ablation speeds and lower deposition temperatures (room temperature), and when DMF or DMSO is used as the perovskite solvent, the perovskite ink does not dry immediately. In order to accelerate the drying of the liquid layer at room temperature, Huang and co-workers introduce about 2% VNCS into the perovskite ink. The VNCS under N_2-knife-assisted blade coating and a mild annealing process gives more time and a lower energy barrier for the perovskite crystalline grains to grow into large sizes and form good contact to the substrate (Fig. 9). By using this method of preparing PSCs, a certified efficiency of 16.4% with an aperture area of 63.7 cm^2 was achieved [29].

B. Additives Engineering

The manufacture of large-area, high-quality, and uniform perovskite films is the main bottleneck for large-area PSCs. In the past decade, there have been a large number of methods for manufacturing large-area perovskite films. Among these methods, the introduction of additives into perovskite precursors has proven to be an effective method for manufacturing large-area and high-quality perovskite films.

1. Organic Halide Ammonium Salts as Additives

Organic halide ammonuim salts (OHAS), both CH_3NH_3 (MA) based and $HC(NH_2)_2$ (FA) based, are the materials that are mostly widely used to improve the morphology of perovskite. Among these OHAS, MACl is considered to be one of the most effective and widely used additives for growth of high-quality perovskite for both small-area and large-area PSCs.

For example, in 2016, Marks and co-workers reported a hot-casting process with controlled Cl^- incorporation that achieves high stability and a high PCE of 15.4% for large-area ($\approx$1 cm^2) single-cell PSC. The enhanced performance can be attributed to the longer carrier diffusion length, the more uniform morphology of perovskite films, the improved perovskite crystallite orientation, and the reduced carrier recombination through the introduction of chloride ions [Fig. 10(a)] [51]. In 2017, Zhu and co-workers used excessive amounts of MACl in perovskite ink, which not only increased the grain size of the perovskite and the crystallinity of the film but also increased the grain growth rate of the perovskite [Fig. 10(b)]. It also significantly reduces thermal annealing requirements. The absorbing layer was prepared by doctor-blade coating. Finally, the average efficiencies of the devices with areas of 1.2 cm^2 and 12.6 cm^2 were 17.33% and 13.3%, respectively [52]. Qi and co-workers introduced MACl into the fast gas-solid reaction of hydrogen

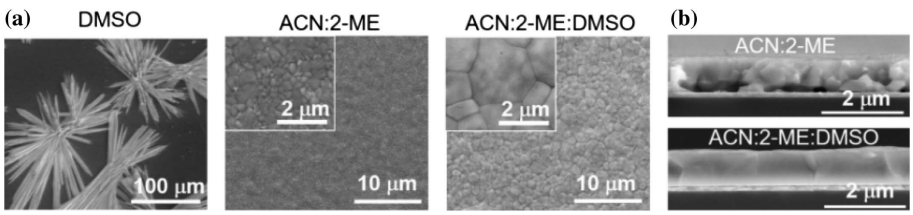

Fig. 9. SEM images of (a) surfaces and (b) cross-sections of perovskite films prepared with different solvents, respectively. Reproduced with permission [29], Copyright 2018, American Association for the Advancement of Science.

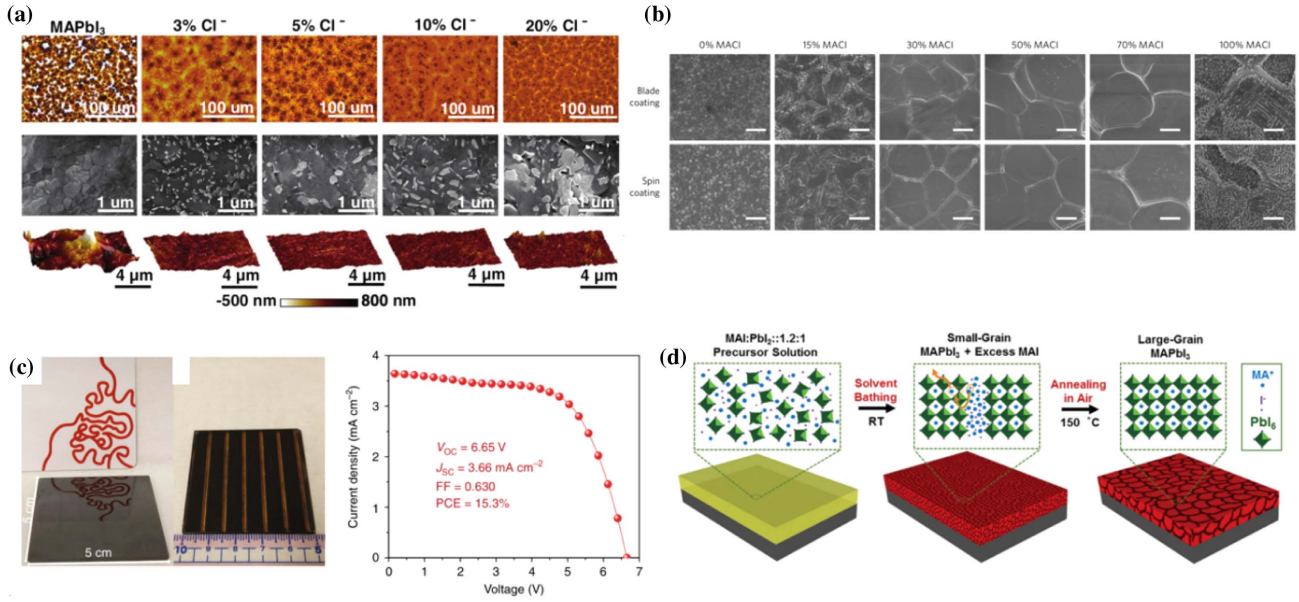

Fig. 10. (a) Morphological characterization of perovskite $MAPbI_3$ films with different amounts of Cl^- incorporation by optical microscopy (top row), SEM (middle row), and atomic force microscope (AFM) (bottom row). (b) Top-view SEM images of perovskite films prepared with different excess amounts of MACl using blade-coating (top row) and spin-coating (bottom row) methods. (c) Photograph of the 1.1 μm thick $MAPbI_3$ (Cl) film on a 5 cm × 5 cm substrate, 12.0 cm^2 six-cell perovskite solar module, and J–V curve of the 5 cm × 5 cm perovskite module with an active area of 12.0 cm^2. (d) Schematic illustration of perovskite film nucleation/crystallization from solvent bathing. (a) Reproduced with permission [51], Copyright 2016, Wiley. (b) Reproduced with permission [52], Copyright 2017, Nature Publishing Group. (c) Reproduced with permission [53], Copyright 2018, Nature Publishing Group. (d) Reproduced with permission [54], Copyright 2015, Wiley.

lead triiodide [$HPbI_3$(Cl)] and CH_3NH_2 gas to fabricate high-quality perovskite films with a thickness of more than 1 μm. The introduction of MACl can not only achieve a small amount of substitution of iodine ions with chlorine ions but also can adjust the morphology of $HPbI_3$ (Cl) films. Finally, a PCE of 15.3% for 5 cm × 5 cm solar modules was achieved [Fig. 10(c)] [53].

When preparing large-area PSCs, $MAPbI_3$ is usually the main component of the perovskite layer. In 2015, Zhu *et al.* found that excess MAI in the perovskite precursor solution also played a positive role in the devices [Fig. 10(d)]. They found that when the excess MAI is absent, the grain size is typically limited to a few hundred nanometers. But when excess MAI is present, it compensates for the loss of any MAI and suppresses (or delays) the formation of a PbI_2 phase during annealing. Using this crystallization-coarsening two-step approach with the nonstoichiometric $MAPbI_3$ precursor solution, the best PCE of 16.3% was achieved for a planar PSC with 1.2 cm^2 active area [54].

2. Inorganic Halide as Additives

In addition to the above-mentioned OHAS as additives that can improve the quality of perovskite films, some inorganic halides are also used as additives into the perovskite to obtain higher-quality perovskite films and improve the PCE of large-area PSCs.

For example, Qiu and co-workers obtained a pinhole-free, highly crystallized perovskite film by introducing $PbCl_2$ into the perovskite precursor and using the one-step spin-coating method followed by thermal annealing for 10 min [Figs. 11(a)–11(d)]. It can be seen from Fig. 11(e) that when 20%–30% $PbCl_2$ is added to the perovskite precursor solution, the pinholes of the perovskite films are the smallest. The high-quality perovskite thin film enables the perovskite module with an area of 4 cm^2 to obtain a PCE of 13.6% [55]. The KI was also introduced into the perovskite precursor by Zhong and co-workers. The incorporation of KI strongly promotes the crystallization of the perovskite film, and its grain size is as high as ∼1 μm [Figs. 11(f)–11(i)], which has doubled compared with those without KI. Perovskite with less interface defect density, longer carrier lifetime, and faster charge transportation was obtained. Finally, a 36 cm^2 submodule with the $K_xCs_{0.05}(FA_{0.85}MA_{0.15})_{0.95}Pb(I_{0.85}Br_{0.15})_3$ (KCsFAMA) composition achieved a high PCE of 15.76% without any hysteresis [56]. In 2019, Qi and co-workers used CsBr additives in FA cationic perovskite manufacturing based on a hybrid chemical vapor deposition (HCVD) process. They achieved a PCE of nearly 10%, and their cell area was 91.8 cm^2 (14 cells in series) [Figs. 11(j) and 11(k)] [57].

3. Other Additives

To fabricate high-efficiency large-area PSCs and solar modules, depositing smooth and uniform perovskite film with full coverage on the substrate is necessary. Huang and co-workers added a small amount L-α-phosphatidylcholine to the $MAPbI_3$/DMF precursor solution and deposited perovskite films via the blade-coating method. They found that the L-α-phosphatidylcholine not only suppressed solution flow but also improved the wettability of the perovskite ink. Through surfactant additive engineering, the authors demonstrated that smooth perovskite films with 14.5 nm root-mean-square roughness could be quickly

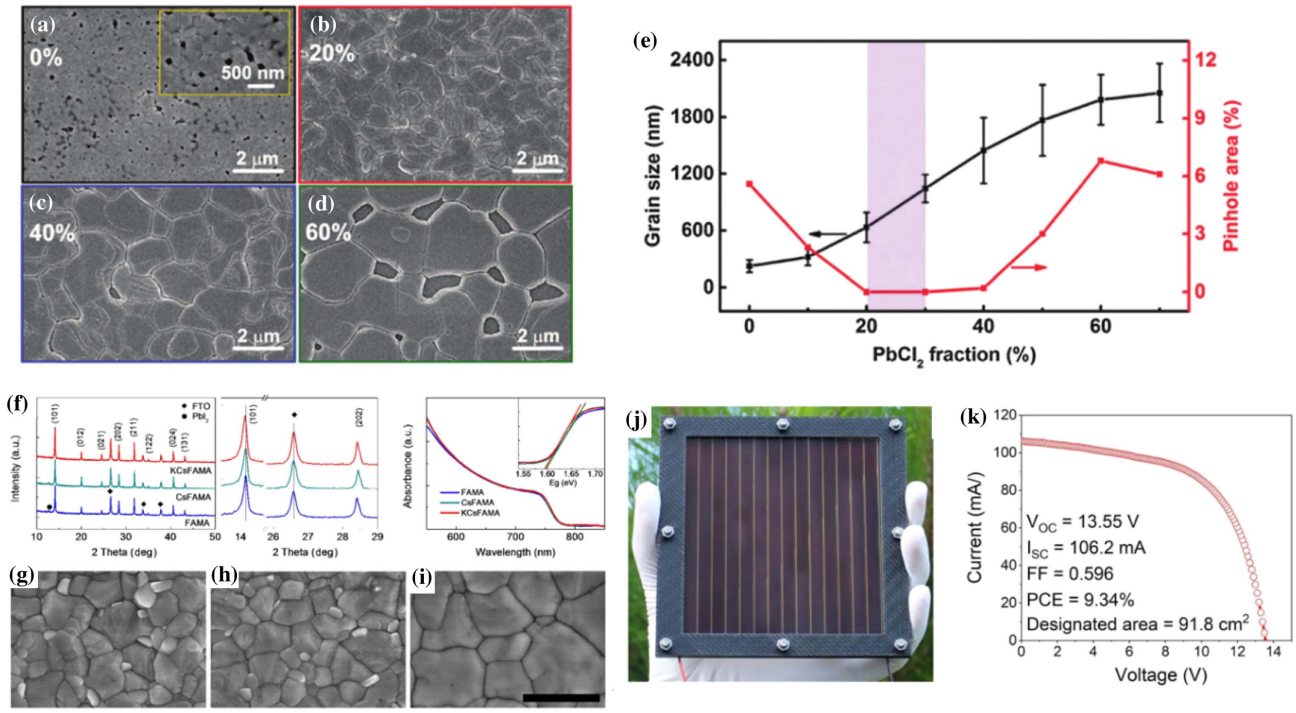

Fig. 11. (a)–(d) Top-view SEM images of perovskite films made with different amounts $PbCl_2$ in the mixed lead source. (e) The crystal grain size and pinhole area in the perovskite films as a function of $PbCl_2$ fraction. (f) XRD patterns and UV-Vis spectra, and (g)–(i) SEM images of FAMA/CsFAMA/KCsFAMA perovskite films, respectively. (j) Optical image of a 10 cm × 10 cm HCVD $Cs_{0.1}FA_{0.9}PbI_{2.9}Br_{0.1}$-based solar module. (k) J-V curve of the champion solar module (14 subcells in series). (a)–(e) Reproduced with permission [55], Copyright 2016, Royal Society of Chemistry. (f)–(i) Reproduced with permission [56], Copyright 2017, Royal Society of Chemistry. (j) and (k) Reproduced with permission [57], Copyright 2019, Royal Society of Chemistry.

deposited by the blade-coating method. Their blade-coated perovskite solar module showed stabilized efficiencies of 15.3% (33.0 cm^2) and 14.6% (57.2 cm^2), respectively [21].

In 2014, Jen *et al.* introduced 1% (mass fraction) 1,8-diiodooctane (DIO) into perovskite precursor solution. The surface of the perovskite films is more continuous and smoother than that obtained from the pristine solution [58]. DIO was also used as an additive to control the growth of perovskite solar modules by Fu *et al.*, and a PCE of 11.2% with an active area over 12 cm^2 was obtained [59].

In addition to the additives mentioned above, some large organic cations and 2D materials have also been introduced as additives in the preparation of large-area high-quality perovskites, which can not only improve the quality of perovskite layer but also improve the stability of perovskites [60–63]. In 2019, Xing *et al.* found that tert-butylammonium (t-BA) in the perovskite precursor solution also played a positive role in the devices, which could not only improve the quality of the perovskite film and increase the carrier diffusion length but also increase the perovskite's stability. By adding t-BA to the perovskite precursor solution, they obtained high-performance PSCs with a champion PCE of 14.54% for area of 20.8 cm^2 [61]. In 2020, the 2D $C_6H_{18}N_2O_2PbI_4$ ($EDBEPbI_4$) was introduced into the precursor solution of perovskite, and the grain boundaries of the deposited 3D perovskite film were vertically passivated with phase-pure 2D perovskite, thereby obtaining a perovskite light-absorbing layer with larger grains and higher stability. By introduction of $EDBEPbI_4$, the PCE of the device has reached 11.59% with an active area of 342 cm^2 [63].

4. FABRICATION OF LARGE-AREA CHARGE TRANSPORTING LAYERS

PSCs are composed of many layers stacked together, including metal electrodes, CTLs, and perovskite layers. As with the preparation of large-area perovskite light-absorbing layers, in addition to spin coating and blade coating, etc., electron beam (E-beam) deposition and chemical bath deposition (CBD) methods are also applied to perovskite solar cells in order to prepare a larger-area, continuous, and high-quality carrier transport layer [64–67]. Many CTLs for small-area PSCs are also used to prepare large-area PSCs, such as TiO_2 [16,52,68,69], SnO_2 [17,70,71], PCBM [28,33,36], NiO [72,73], Spiro-OMeTAD [17,30,34,35,44,45], and PTAA [37]. In this section, we briefly summarize the other works on CTLs in PSCs.

In 2015, Han and co-workers prepared efficient and stable large-area PSCs with inorganic CTLs, and they obtained a PCE beyond 15% with an area beyond 1 cm^2 [Fig. 12(b)]. They used p-doped (p^+) $Ni_xMg_{1-x}O$ and n-doped (n^+) TiO_x contacts to selectively extract charge carriers from inverted PSCs. They implemented the p^+ and n^+ doping by substituting $Ni(Mg)^{2+}$ ions and Ti^{4+} ions on the $Ni_xMg_{1-x}O$ lattice and TiO_x matrix by Li^+ and Nb^{5+} ions, respectively [Fig. 12(a)]. The PSCs with the inorganic CTLs were stable: beyond 90% of

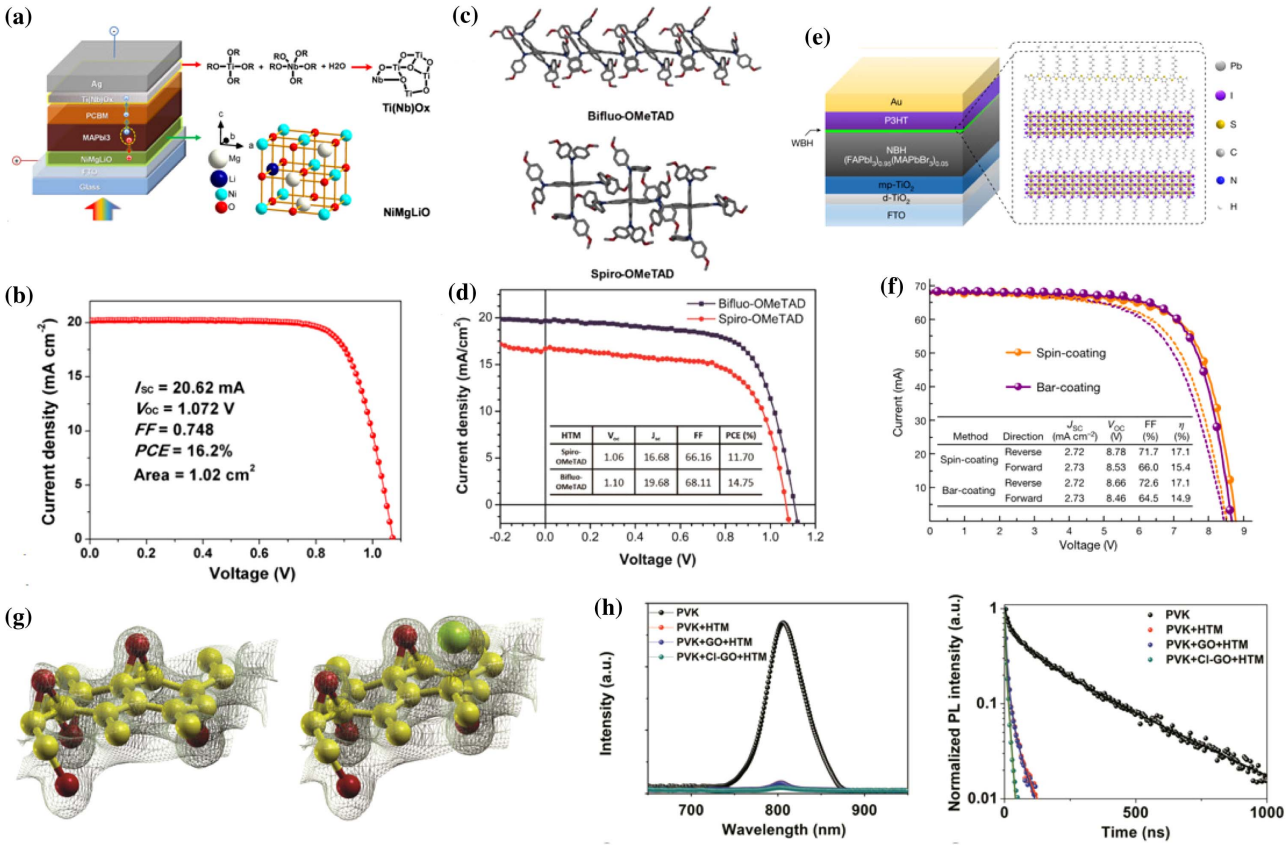

Fig. 12. (a) Scheme of the cell configuration highlighting the doped charge carrier extraction layers. (b) J–V curve of the best large cell endowed with antireflection film. (c) Comparison of the Bifluo-OMeTAD molecule (upper) and Spiro-OMeTAD (Merck) molecule. (d) J-V curve of PSCs with HTLs Bifluo-OMeTAD and Spiro-OMeTAD. (e) The structure of using P3HT as the HTL and structure of the interface between the P3HT and WBH. (f) I-V curves of solar modules formed by depositing the P3HT layer using bar-coating (purple) and spin-coating (orange) methods. (g) The DFT simulation of GO and Cl-GO. (h) PL spectra and TRPL spectra for different films. (a) and (b) Reproduced with permission [19], Copyright 2017, Wiley. (c) and (d) Reproduced with permission [74], Copyright 2017, Nature Publishing Group. (e) and (f) Reproduced with permission [75], Copyright 2019, Nature Publishing Group. (g) and (h) Reproduced with permission [76], Copyright 2019, American Association for the Advancement of Science.

the initial PCE was maintained after 1000 hours of light soaking [19].

Spiro-OMeTAD is an excellent HTL in the small-area PSCs, while using it in large-area PSCs by the slot-die coating technology will cause a significant decrease in performance due to crystallization. In this regard, Cheng and co-workers designed a new HTL (Bifluo-OMeTAD) [Fig. 12(c)]. This molecular arrangement could suppress crystallization during deposition, and a PCE of 14.7% was achieved with the Bifluo-OMeTAD as the HTL, which is higher than that of the devices based on Spiro-OMeTAD as the HTL [Fig. 12(d)] [74]. In addition to the HTLs of Spiro-OMeTAD and PTAA, P3HT is also used in large-area PSCs, and some progress has been made. Vak and co-workers used P3HT as the HTL through slot-die coating technology, and they obtained a PCE of 11.94% for PSCs in 2015 [32]. Despite the potential advantages of P3HT, the open circuit voltage (V_{oc}) of the resulting device is lower due to the nonradiative recombination that occurs at the perovskite/P3HT interface. At the same time, the electronic coupling between the perovskite and P3HT molecule will also result in low electrical coupling. To address these issues, Seo *et al.* applied an ultrathin wide-bandgap halide (WBH) perovskite layer on top of the narrow-bandgap light-absorbing layer [(Fig. 12(e)]. The purpose of adding the WBH layer in the perovskite/P3HT interface is to effectively reduce recombination. They found that when P3HT is deposited on the surface of the WBH, interdigitation of its alkyl chains and the analogous alkyl chains of n-hexyltrimethyl ammonium bromide (C_6H_{13}-) should promote the self-assembly of P3HT. By this method, an average PCE of 16.0% was obtained for large-area module (24.97 cm^2) PSCs [Fig. 12(f)] [75].

Han and co-workers also introduced a chlorinated graphene oxide (Cl-GO) layer between the perovskite and the HTL. The heterostructure consists of a Pb-rich perovskite film and a Cl-GO layer, forming strong Pb-Cl and P-O bonds to connect the two layers. They compared the perovskite/PTAA with the perovskite/GO/PTAA samples; the perovskite/Cl-GO/PTAA sample exhibited the lowest steady-state photoluminescence (PL) signal, consistent with transient photoluminescence (TRPL) results. The results indicated that reduced charge recombination and more efficient charge extraction occurred in the perovskite/Cl-GO/PTAA heterostructure [Figs. 12(g)

and 12(h)]. The PCE of PSCs with an aperture area of 1.02 cm^2 was about 21% [76].

5. OUTLOOK AND SUMMARY

In this review, we have summarized recent progress in large-area perovskite solar cells, including the perovskite film deposition method and also how to control the growth of large-area, high-quality perovskite films and charge transport layers. Although there is significant progress in large-area perovskite solar cells, and the efficiency has been beyond 18% and 16% for around 20 cm^2 and 800 cm^2, respectively, there is still a certain efficiency gap between the large and small size. Therefore, it is still important to improve the PCE of PSCs for large-area devices. We believe the perovskite film itself is critical for delivering high efficiency of large-area PSCs, and there could be three directions. (i) The first approach should be the most important: we need to find a deposition method and also a perfect precursor for deposition of large crystal perovskite films, free of cracks and pinholes, that reduces the bulk defect recombination. (ii) Composition engineering: most of the works on large-area PSCs are focused on $MAPbI_3$ with a large bandgap, and we should adjust the perovskite bandgap to be smaller. (iii) The third approach is interface modification, which reduces interface defects and the charge recombination; in addition, the electrical contact is also important.

In addition to improving the PCE of PSCs, for commercial development of PSCs, the stability is another challenge that urgently needs to be addressed. The longest lifetime reported for small-area PSCs is about one year [77], which is much shorter than the 25 years of commercialized PV technologies [50]. Besides, while enlarging the device area, the lateral contact between metal and perovskite could reduce the lifetime. Factors affecting the stability of PSCs include: the unstable chemical composition of perovskite; the charge transport material and interfacial degradation; metal electrodes suffering from corrosion by ion migration in perovskite; and the external environment, such as water, oxygen, heat, and light. The hygroscopicity of PSCs can be solved by encapsulation technology. It is necessary to adjust the composition, reduce defects, and select an HTL with high carrier mobility and conductivity to solve the problems of PSCs' thermal instability and ion migration. On the other hand, the ion migration is almost unavoidable in PSCs, and the situation is worse at the defective sites, grain boundaries, and the interfaces of the PSCs [50]. Unlike small-area PSCs, currently, in large-area PSC modules, the passivation layer is rarely used to passivate surface defects on the perovskite surface. As a result, a kind of passivation film that can form a large, uniform area and passivate the surface of the perovskite should be developed and then used to improve the performance of the modules. We believe that we can obtain more high-performance and stable, large-area PSCs by optimizing the preparation method for large-area modules, growing high-quality perovskite thin films, reducing the number of carrier recombination centers in the devices, and choosing the appropriate CTLs.

Funding. China National Funds for Distinguished Young Scientists (61925405).

Disclosures. The authors declare no conflicts of interest.

REFERENCES

1. K. Kojima, Y. Teshima, T. Shirai, and T. Miyasaka, "Organometal halide perovskites as visible-light sensitizers for photovoltaic cells," J. Am. Chem. Soc. **131**, 6050–6051 (2009).
2. H. Kim, C. Lee, J. H. Im, K. Lee, T. Moehl, A. Marchioro, S. Moon, R. Humphry-Baker, J. Yum, J. Moser, M. Gratzel, and N. Park, "Lead iodide perovskite sensitized all-solid-state submicron thin film mesoscopic solar cell with efficiency exceeding 9%," Sci. Rep. **2**, 591 (2012).
3. M. M. Lee, J. Teuscher, T. Miyasaka, T. N. Murakami, and H. J. Snaith, "Efficient hybrid solar cells based on meso-superstructured organometal halide perovskites," Science **338**, 643–647 (2012).
4. W. Yang, J. Noh, N. Jeon, Y. Kim, S. Ryu, J. Seo, and S. Seok, "High-performance photovoltaic perovskite layers fabricated through intramolecular exchange," Science **348**, 1234–1237 (2015).
5. D. Bi, C. Yi, J. Luo, J. D. Decoppet, F. Zhang, S. Zakeeruddin, X. Li, A. Hagfeldt, and M. Gratzel, "Polymer-templated nucleation and crystal growth of perovskite films for solar cells with efficiency greater than 21%," Nat. Energy **1**, 16142 (2016).
6. W. S. Yang, B.-W. Park, E. H. Jung, N. J. Jeon, Y. C. Kim, D. Uk Lee, S. S. Shin, J. Seo, E. K. Kim, J. H. Noh, and S. Il Seok, "Iodide management in formamidinium-lead-halide-based perovskite layers for efficient solar cells," Science **356**, 1376–1379 (2017).
7. N. Jeon, H. Na, E. Jung, T.-Y. Yang, Y. Lee, G. Kim, H.-W. Shin, S. Seok, J. Lee, and J. Seo, "A fluorene-terminated hole-transporting material for highly efficient and stable perovskite solar cells," Nat. Energy **3**, 682–689 (2018).
8. Q. Jiang, Y. Zhao, X. Zhang, X. Yang, Y. Chen, Z. Chu, Q. Ye, X. Li, Z. Yin, and J. You, "Surface passivation of perovskite film for efficient solar cells," Nat. Photonics **13**, 460–466 (2019).
9. https://www.nrel.gov/pv/assets/pdfs/best-research-cell-efficiencies.20200218.pdf.
10. Q. Ye, Y. Zhao, S. Mu, P. Gao, X. Zhang, and J. You, "Stabilizing the black phase of cesium lead halide inorganic perovskite for efficient solar cells," Sci. China Chem. **62**, 810–821 (2019).
11. F. Gao, Y. Zhao, X. Zhang, and J. You, "Recent progresses on defect passivation toward efficient perovskite solar cells," Adv. Energy Mater. **10**, 1902650 (2019).
12. J.-W. Lee, D.-K. Lee, D.-N. Jeong, and N.-G. Park, "Control of crystal growth toward scalable fabrication of perovskite solar cells," Adv. Funct. Mater. **29**, 1807047 (2018).
13. D. H. Kim, J. B. Whitaker, Z. Li, M. F. A. M. van Hest, and K. Zhu, "Outlook and challenges of perovskite solar cells toward terawatt-scale photovoltaic module technology," Joule **2**, 1437–1451 (2018).
14. N.-G. Park, "Research direction toward scalable, stable, and high efficiency perovskite solar cells," Adv. Energy Mater. **10**, 1903106 (2019).
15. B. Cao, L. Yang, S. Jiang, H. Lin, N. Wang, and X. Li, "Flexible quintuple cation perovskite solar cells with high efficiency," J. Mater. Chem. A **7**, 4960–4970 (2019).
16. T. Bu, J. Li, F. Zheng, W. Chen, X. Wen, Z. Ku, Y. Peng, J. Zhong, Y.-B. Cheng, and F. Huang, "Universal passivation strategy to slot-die printed SnO_2 for hysteresis-free efficient flexible perovskite solar module," Nat. Commun. **9**, 4609 (2018).
17. W. Chen, Y. Wu, Y. Yue, J. Liu, W. Zhang, X. Yang, H. Chen, E. Bi, I. Ashraful, M. Grätzel, and L. Han, "Efficient and stable large-area perovskite solar cells with inorganic charge extraction layers," Science **350**, 944–948 (2015).
18. H. Tan, A. Jain, O. Voznyy, X. Lan, F. P. G. de Arquer, J. Z. Fan, R. Q. Bermudez, M. Yuan, B. Zhang, Y. Zhao, F. Fan, P. Li, L. N. Quan, Y. Zhao, Z.-H. Lu, Z. Yang, S. Hoogland, and E. H. Sargent, "Efficient and stable solution-processed planar perovskite solar cells via contact passivation," Science **355**, 722–726 (2017).
19. Q. Jiang, Z. Chu, P. Wang, X. Yang, H. Liu, Y. Wang, Z. Yin, J. Wu, X. Zhang, and J. You, "Planar-structure perovskite solar cells with efficiency beyond 21%," Adv. Mater. **29**, 1703852 (2017).

20. Y. Deng, E. Peng, Y. Shao, Z. Xiao, Q. Dong, and J. Huang, "Scalable fabrication of efficient organolead trihalide perovskite solar cells with doctor-bladed active layers," Energy Environ. Sci. **8**, 1544–1550 (2015).
21. Y. Deng, X. Zheng, Y. Bai, Q. Wang, J. Zhao, and J. Huang, "Surfactant-controlled ink drying enables high-speed deposition of perovskite films for efficient photovoltaic modules," Nat. Energy **3**, 560–566 (2018).
22. H. Chen, F. Ye, W. Tang, J. He, M. Yin, Y. Wang, F. Xie, E. Bi, X. Yang, M. Grätzel, and L. Han, "A solvent- and vacuum-free route to large-area perovskite films for efficient solar modules," Nature **550**, 92–95 (2017).
23. http://www.microquanta.com/.
24. M. A. Green, E. D. Dunlop, J. H. Ebinger, M. Yoshita, N. Kopidakis, and A. W. Y. Ho-Baillie, "Solar cell efficiency tables (version 55)," Prog. Photovolt. Res. Appl. **28**, 3–15 (2020).
25. H. S. Jung, G. S. Han, N.-G. Park, and M. J. Ko, "Flexible perovskite solar cells," Joule **3**, 1850–1880 (2019).
26. Y. Chen, L. Zhang, Y. Zhang, H. Gao, and H. Yan, "Large-area perovskite solar cells – a review of recent progress and issues," RSC Adv. **8**, 10489–10508 (2018).
27. N. J. Jeon, J. H. Noh, W. S. Yang, Y. C. Kim, S. Ryu, J. Seo, and S. Il Seok, "Compositional engineering of perovskite materials for high-performance solar cells," Nature **517**, 476–480 (2015).
28. Z. Yang, C.-C. Chueh, F. Zuo, J. H. Kim, P.-W. Liang, and A. K.-Y. Jen, "High-performance fully printable perovskite solar cells via blade-coating technique under the ambient condition," Adv. Energy Mater. **5**, 1500328 (2015).
29. Y. Deng, C. H. V. Brackle, X. Dai, J. Zhao, B. Chen, and J. Huang, "Tailoring solvent coordination for high-speed, room-temperature blading of perovskite photovoltaic films," Sci. Adv. **5**, eaax7537 (2019).
30. J. B. Whitaker, D. H. Kim, B. W. Larson, F. Zhang, J. J. Berry, M. F. A. M. van Hest, and K. Zhu, "Scalable slot-die coating of high performance perovskite solar cells," Sustain. Energy Fuels **2**, 2442–2449 (2018).
31. D. Vak, K. Hwang, A. Faulks, Y.-S. Jung, N. Clark, D.-Y. Kim, G. J. Wilson, and S. E. Watkins, "3D printer based slot-die coater as a lab-to-fab translation tool for solution-processed solar cells," Adv. Energy Mater. **5**, 1401539 (2014).
32. K. Hwang, Y.-S. Jung, Y.-J. Heo, F. H. Scholes, S. E. Watkins, J. Subbiah, D. J. Jones, D.-Y. Kim, and D. Vak, "Toward large scale roll-to-roll production of fully printed perovskite solar cells," Adv. Mater. **27**, 1241–1247 (2015).
33. C. Zuo, D. Vak, D. Angmo, L. Ding, and M. Gao, "One-step roll-to-roll air processed high efficiency perovskite solar cells," Nano Energy **46**, 185–192 (2018).
34. F. D. Giacomo, S. Shanmugam, H. Fledderus, B. J. Bruijnaers, W. J. Verhees, M. S. Dorenkamper, S. C. Veenstra, W. Qiu, R. Gehlhaar, and T. Merckx, "Up-scalable sheet-to-sheet production of high efficiency perovskite module and solar cells on 6-in. substrate using slot die coating," Sol. Energy Mater. Sol. Cells **181**, 53–59 (2018).
35. J. G. Tait, S. Manghooli, W. Qiu, L. Rakocevic, L. Kootstra, M. Jaysankar, C. A. Massede la Huerta, U. W. Paetzold, R. Gehlhaar, D. Cheyns, P. Heremans, and J. Poortmans, "Rapid composition screening for perovskite photovoltaics via concurrently pumped ultrasonic spray coating," J. Mater. Chem. A **4**, 3792–3797 (2016).
36. A. T. Barrows, A. J. Pearson, C. K. Kwak, A. D. F. Dunbar, A. R. Buckley, and D. G. Lidzey, "Efficient planar heterojunction mixed-halide perovskite solar cells deposited via spray-deposition," Energy Environ. Sci. **7**, 2944–2950 (2014).
37. J. H. Heo, M. H. Lee, M. H. Jang, and S. H. Im, "Highly efficient $CH_3NH_3PbI_{3-x}Cl_x$ mixed halide perovskite solar cells prepared by re-dissolution and crystal grain growth via spray coating," J. Mater. Chem. A **4**, 17636–17642 (2016).
38. M. Park, W. Cho, G. Lee, S. C. Hong, M.-C. Kim, J. Yoon, N. Ahn, and M. Choi, "Highly reproducible large-area perovskite solar cell fabrication via continuous megasonic spray coating of $CH_3NH_3PbI_3$," Small **15**, 1804005 (2018).
39. O. A. Basaran, H. Gao, and P. P. Bhat, "Nonstandard inkjets," Annu. Rev. Fluid Mech. **45**, 85–113 (2013).
40. S. K. Karunakaran, G. M. Arumugam, W. Yang, S. Ge, S. N. Khan, X. Lin, and G. Yang, "Recent progress in inkjet-printed solar cells," J. Mater. Chem. A **7**, 13873–13902 (2019).
41. A. Priyadarshi, L. J. Haur, P. Murray, D. Fu, S. Kulkarni, G. Xing, T. C. Sum, N. Mathews, and S. G. Mhaisalkar, "A large area (70 cm^2) monolithic perovskite solar module with a high efficiency and stability," Energy Environ. Sci. **9**, 3687–3692 (2016).
42. C. Liang, P. Li, H. Gu, Y. Zhang, F. Li, Y. Song, G. Shao, N. Mathews, and G. Xing, "One-step inkjet printed perovskite in air for efficient light harvesting," Sol. RRL **2**, 1700217 (2018).
43. P. Li, C. Liang, B. Bao, Y. Li, X. Hu, Y. Wang, Y. Zhang, F. Li, G. Shao, and Y. Song, "Inkjet manipulated homogeneous large size perovskite grains for efficient and large-area perovskite solar cells," Nano Energy **46**, 203–211 (2018).
44. J.-E. Kim, S.-S. Kim, C. Zuo, M. Gao, D. Vak, and D.-Y. Kim, "Humidity-tolerant roll-to-roll fabrication of perovskite solar cells via polymer-additive- assisted hot slot die deposition," Adv. Funct. Mater. **29**, 1809194 (2019).
45. Y. Y. Kim, T.-Y. Yang, R. Suhonen, M. Välimäki, T. Maaninen, A. Kemppainen, N. J. Jeon, and J. Seo, "Gravure-printed flexible perovskite solar cells: toward roll-to-roll manufacturing," Adv. Sci. **6**, 1802094 (2019).
46. X. Li, D. Bi, C. Yi, J.-D. Décoppet, J. Luo, S. M. Zakeeruddin, A. Hagfeldt, and M. Grätzel, "A vacuum flash-assisted solution process for high-efficiency large-area perovskite solar cells," Science **353**, 58–62 (2016).
47. Y. Rong, Y. Hu, A. Mei, H. Tan, M. I. Saidaminov, S. Il Seok, M. D. McGehee, E. H. Sargent, and H. Han, "Challenges for commercializing perovskite solar cells," Science **361**, eaat8235 (2018).
48. Y. Zhao, Q. Ye, Z. Chu, F. Gao, X. Zhang, and J. You, "Recent progress in high-efficiency planar-structure perovskite solar cells," Energy Environ. Mater. **2**, 93–106 (2019).
49. Y. Wu, A. Islam, X. Yang, C. Qin, J. Liu, K. Zhang, W. Peng, and L. Han, "Retarding the crystallization of PbI_2 for highly reproducible planar-structured perovskite solar cells via sequential deposition," Energy Environ. Sci. **7**, 2934–2938 (2014).
50. N. J. Jeon, J. H. Noh, Y. C. Kim, W. S. Yang, S. Ryu, and S. I. Seok, "Solvent engineering for high-performance inorganic-organic hybrid perovskite solar cells," Nat. Mater. **13**, 897–903 (2014).
51. H.-C. Liao, P. Guo, C.-P. Hsu, M. Lin, B. Wang, L. Zeng, W. Huang, C. M. M. Soe, W.-F. Su, M. J. Bedzyk, M. R. Wasielewski, A. Facchetti, R. P. H. Chang, M. G. Kanatzidis, and T. J. Marks, "Enhanced efficiency of hot-cast large-area planar perovskite solar cells/modules having controlled chloride incorporation," Adv. Energy Mater. **7**, 1601660 (2017).
52. M. Yang, Z. Li, M. O. Reese, O. G. Reid, D. H. Kim, S. Siol, T. R. Klein, Y. Yan, J. J. Berry, M. F. A. M. van Hest, and K. Zhu, "Perovskite ink with wide processing window for scalable high-efficiency solar cells," Nat. Energy **2**, 17038 (2017).
53. Z. Liu, L. Qiu, E. J. J. Perez, Z. Hawash, T. Kim, Y. Jiang, Z. Wu, S. R. Raga, L. K. Ono, S. F. Liu, and Y. Qi, "Gas-solid reaction based over one-micrometer thick stable perovskite films for efficient solar cells and modules," Nat. Commun. **9**, 3880 (2018).
54. M. Yang, Y. Zhou, Y. Zeng, C.-S. Jiang, N. P. Padture, and K. Zhu, "Square-centimeter solution-processed planar $CH_3NH_3PbI_3$ perovskite solar cells with efficiency exceeding 15%," Adv. Mater. **27**, 6363–6370 (2015).
55. W. Qiu, T. Merckx, M. Jaysankar, C. Masse de la Huerta, L. Rakocevic, W. Zhang, U. W. Paetzold, R. Gehlhaar, L. Froyen, J. Poortmans, D. Cheyns, H. J. Snaith, and P. Heremans, "Pinhole-free perovskite films for efficient solar modules," Energy Environ. Sci. **9**, 484–489 (2016).
56. T. Bu, X. Liu, Y. Zhou, J. Yi, X. Huang, L. Luo, J. Xiao, Z. Ku, Y. Peng, F. Huang, Y.-B. Cheng, and J. Zhong, "Novel quadruple-cation absorber for universal hysteresis elimination for high efficiency and stable perovskite solar cells," Energy Environ. Sci. **10**, 2509–2515 (2017).
57. L. Qiu, S. He, Y. Jiang, D.-Y. Son, L. K. Ono, Z. Liu, T. Kim, T. Bouloumis, S. Kazaoui, and Y. Qi, "Hybrid chemical vapor deposition

enables scalable and stable Cs-FA mixed cation perovskite solar modules with a designated area of 91.8 cm^2 approaching 10% efficiency," J. Mater. Chem. A **7**, 6920–6929 (2019).
58. P.-W. Liang, C.-Y. Liao, C.-C. Chueh, F. Zuo, S. T. Williams, X.-K. Xin, J. Lin, and A. K.-Y. Jen, "Additive enhanced crystallization of solution-processed perovskite for highly efficient planar-heterojunction solar cells," Adv. Mater. **26**, 3748–3754 (2014).
59. G. Fu, L. Hou, Y. Wang, X. Liu, J. Wang, H. Li, Y. Cui, D. Liu, X. Li, and S. Yang, "Efficiency enhancement in planar $CH_3NH_3PbI_{3-x}Cl_x$ perovskite solar cells by processing with bidentate halogenated additives," Sol. Energy Mater. Sol. Cells **165**, 36–44 (2017).
60. C. Liang, D. Zhao, Y. Li, X. Li, S. Peng, G. Shao, and G. Xing, "Ruddlesden–Popper perovskite for stable solar cells," Energy Environ. Mater. **1**, 221–231 (2018).
61. C. Liang, D. Zhao, P. Li, B. Wu, H. Gu, J. Zhang, T. W. Goh, S. Chen, Y. Chen, Z. Sha, G. Shao, T. C. Sumb, and G. Xing, "Simultaneously boost diffusion length and stability of perovskite for high performance solar cells," Nano Energy **59**, 721–729 (2019).
62. C. Liang, K. M. Muhammed Salim, P. Li, Z. Wang, T. M. Koh, H. Gu, B. Wu, J. Xia, Z. Zhang, K. Wang, T. Liu, Q. Wei, S. Wang, Y. Tang, G. Shao, Y. Song, N. Mathews, and G. Xing, "Controlling films structure by regulating 2D Ruddlesden-Popper perovskite formation enthalpy for efficient and stable tri-cation perovskite solar cells," J. Mater. Chem. A **8**, 5874–5881 (2020).
63. P. Li, Y. Zhang, C. Liang, G. Xing, X. Liu, F. Li, X. Liu, X. Hu, G. Shao, and Y. Song, "Phase pure 2D perovskite for high-performance 2D-3D heterostructured perovskite solar cells," Adv. Mater. **30**, 1805323 (2018).
64. J. Feng, Z. Yang, D. Yang, X. Ren, X. Zhu, Z. Jin, W. Zi, Q. Wei, and S. F. Liu, "E-beam evaporated Nb_2O_5 as an effective electron transport layer for large flexible perovskite solar cells," Nano Energy **36**, 1–8 (2017).
65. C. Liang, Z. Wu, P. Li, J. Fan, Y. Zhang, and G. Shao, "Making high-quality CTLs is as important as making high-quality perovskite films to achieve efficient and stable PSCs," Appl. Surf. Sci. **391**, 337–341 (2017).
66. J. Sun, J. Lu, B. Li, L. Jiang, A. S. R. Chesman, A. D. Scully, T. R. Gengenbach, Y.-B. Cheng, and J. J. Jasieniak, "Inverted perovskite solar cells with high fill-factors featuring chemical bath deposited mesoporous NiO hole transporting layers," Nano Energy **49**, 163–171 (2018).
67. X. Ren, L. Xie, W. B. Kim, D. G. Lee, H. S. Jung, and S. F. Liu, "Chemical bath deposition of co-doped TiO_2 electron transport layer for hysteresis-suppressed high-efficiency planar perovskite solar cells," Sol. RRL **3**, 1900176 (2019).
68. A. Mei, X. Li, L. Liu, Z. Ku, T. Liu, Y. Rong, M. Xu, M. Hu, J. Chen, Y. Yang, M. Grätzel, and H. Han, "A hole-conductor-free, fully printable mesoscopic perovskite solar cell with high stability," Science **345**, 295–298 (2014).
69. Y. Hu, S. Si, A. Mei, Y. Rong, H. Liu, X. Li, and H. Han, "Stable large-area (10×10 cm^2) printable mesoscopic perovskite module exceeding 10% efficiency," Sol. RRL **1**, 1600019 (2017).
70. B. Dou, J. B. Whitaker, K. Bruening, D. T. Moore, L. M. Wheeler, J. Ryter, N. J. Breslin, J. J. Berry, S. M. Garner, and F. Barnes, "Roll-to-roll printing of perovskite solar cells," ACS Energy Lett. **3**, 2558–2565 (2018).
71. L. Qiu, Z. Liu, L. K. Ono, Y. Jiang, D.-Y. Son, Z. Hawash, S. He, and Y. Qi, "Scalable fabrication of stable high efficiency perovskite solar cells and modules utilizing room temperature sputtered SnO_2 electron transport layer," Adv. Funct. Mater. **29**, 1806779 (2019).
72. G. Li, Y. Jiang, S. Deng, A. Tam, P. Xu, M. Wong, and H.-S. Kwok, "Overcoming the limitations of sputtered nickel oxide for high-efficiency and large-area perovskite solar cells," Adv. Sci. **4**, 1700463 (2017).
73. W. Chen, Y. Wu, J. Fan, A. B. Djurišić, F. Liu, H. W. Tam, A. Ng, C. Surya, W. K. Chan, D. Wang, and Z.-B. He, "Understanding the doping effect on NiO: toward high-performance inverted perovskite solar cells," Adv. Energy Mater. **8**, 1703519 (2018).
74. T. Qin, W. Huang, J.-E. Kim, D. Vak, C. Forsyth, C. R. McNeill, and Y.-B. Cheng, "Amorphous hole-transporting layer in slot-die coated perovskite solar cells," Nano Energy **31**, 210–217 (2017).
75. E. H. Jung, N. J. Jeon, E. Y. Park, C. S. Moon, T. J. Shin, T.-Y. Yang, J. H. Noh, and J. Seo, "Efficient, stable and scalable perovskite solar cells using poly(3-hexylthiophene)," Nature **567**, 511–515 (2019).
76. Y. Wang, T. Wu, J. Barbaud, W. Kong, D. Cui, H. Chen, X. Yang, and L. Han, "Stabilizing heterostructures of soft perovskite semiconductors," Science **365**, 687–691 (2019).
77. G. Grancini, C. Roldán-Carmona, I. Zimmermann, E. Mosconi, X. Lee, D. Martineau, S. Narbey, F. Oswald, F. De Angelis, M. Graetzel, and M. K. Nazeeruddin, "One-year stable perovskite solar cells by 2D/3D interface engineering," Nat. Commun. **8**, 15684 (2017).